



Impact of Pulsed Laser Parameters and Scanning Pattern on the Properties of Thin-Walled Parts Manufactured Using Laser Metal Deposition

Weiwei Liu¹ · Gamal Al-Hammadi¹ · Kazi Mojtaba Saleheen¹ · Ahmed Abdelrahman¹ · Huanqiang Liu¹ · Zhidong Zhang²

Received: 21 May 2022 / Revised: 26 July 2022 / Accepted: 3 August 2022 / Published online: 2 November 2022

© The Author(s) 2022

Abstract

The quality of parts manufactured using laser metal deposition (LMD), similar to other additive manufacturing methods, is influenced by processing parameters. Such parameters determine geometric stability, favorable microstructures, and good mechanical properties. This study aimed to investigate the effects of pulsed laser parameters (duty cycle and pulse frequency) and scanning patterns (unidirectional and bidirectional patterns) on the properties of parts fabricated using LMD. Results show that the properties of the LMD-fabricated parts are obviously influenced by pulsed laser parameters and scanning patterns. Using the unidirectional scanning pattern in both pulsed laser parameters enhances the properties of the thin-walled parts prepared using LMD. An increase in duty cycle can improve geometric stability, increase grain size, and reduce microhardness. Furthermore, the geometric stability does not vary considerably with the use of different frequencies, but the microstructure of fabricated parts shows various grain sizes with different pulse frequencies. In addition, the microhardness increases as the frequency increases from 13.33 to 50 Hz. In general, the influence of the duty cycle on geometric properties is greater than that of frequency. Meanwhile, the impact of frequency on microhardness is greater than that of the duty cycle.

Keywords Laser metal deposition (LMD) · Pulse laser · Scanning pattern · Geometric properties · Grain size · Hardness

1 Introduction

Laser metal deposition (LMD) is the most common type of directed energy deposition (DED) technology that uses a laser to fabricate high-strength, short-duration metal components directly from a computer-aided design (CAD) model without the use of molds [1]. As shown in Fig. 1, LMD uses laser power as a heat source to melt the substrate, and the raw materials are fed into the molten pool in the form of metal wire or powder. A single track is formed with the movement of the laser beam, and then a 3D part is formed as this movement is continued layer upon layer [2, 3]. LMD is superior to traditional technologies in terms of geometric

freedom, production flexibility, and low thermal input; thus, it has attracted considerable attention in the fields of aerospace, aviation, and mold as an effective and efficient process to fabricate metal and cladding parts and repair and refurbish damaged parts [4, 5].

Although LMD is an important technique for manufacturing, repairing, and refurbishing damaged components, its lack of consistent and reliable quality limits its applications. Several scholars have analyzed the influence of LMD process parameters, including laser power, scanning speed, and powder flow rate, on the properties of the fabricated or remanufactured parts to increase the quality and reliability of these parts. Riquelme et al. [6] have investigated the influence of laser power and scanning speed on the microstructure of Al/SiCp composites during LMD and evaluated the wear behavior and microhardness of the fabricated parts. Eo et al. [2] have studied the effects of the melt pool oxidation and inclusion characteristics of LMD 316L stainless steel on the mechanical properties and their relation to laser power, scanning speed, and powder chemistry. Xiang et al. [7] compared the microstructures and mechanical properties

✉ Weiwei Liu
liuww@dlut.edu.cn

¹ School of Mechanical Engineering, Dalian University of Technology, Dalian 116024, China

² Liaoshen Industries Group Co., Ltd, Shenyang 110041, China

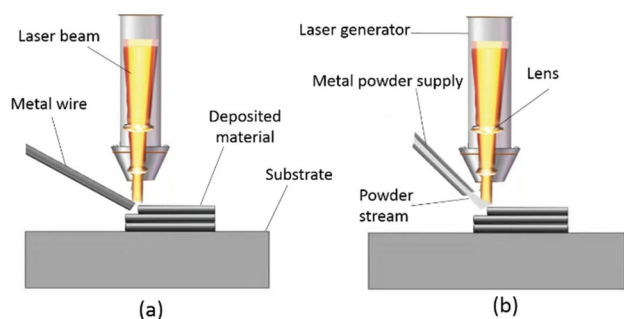


Fig. 1 Schematic of LMD: **a** wire feeding and **b** powder feeding

of CrMnFeCoNi prepared using LMD and casting methods. The results showed that the samples prepared using LMD contain columnar and equiaxed grains and that the proportion of these grain structures can be modified by changing the laser power, whereas those prepared through casting possess a coarse dendritic structure. In addition, the mechanical properties of the 1400-W samples prepared using LMD are better than those prepared using casting. Xue et al. [8] investigated the mechanism by which various laser energy densities affect the microstructure and microhardness of fabricated parts during LMD. They found that a decrease in laser energy density (LED) can alter the microstructure of the parts, decrease their sub-grain size, and increase their microhardness.

Numerous studies have focused on improving the properties of fabricated parts during LMD by controlling the process parameters in a continuous-wave laser. However, the effects of pulsed laser parameters on these properties remain unclear despite their significant effect on the microstructure and mechanical properties of parts prepared using LMD [9–13]. The scanning pattern also considerably influences the fine structure and mechanical properties of parts manufactured via LMD using continuous-wave lasers [14–20], but its effects when pulse wave lasers are used remain to be determined. Gharbi et al. [9] investigated the effects of pulsed laser parameters on the surface finish caused by LMD on titanium alloy (Ti6Al4V). They demonstrated that high mean power enhances surface quality, and the usage of a pulsed mode with several duty cycles provides clear smoothening effects. Li et al. [10] found that the microstructure during pulsed laser processing shows finer columnar dendrites than that during continuous laser processing. In addition, the dendrite development direction is more oriented toward the laser scanning direction than the continuous laser power sample. Pinkerton et al. [11] found that pulsed laser may reduce the porosity of fabricated parts more during LMD than during continuous laser processing. Ravi et al. [12] found that laser mode and laser power significantly affect the grain structure. The continuous-wave mode usually leads to large columnar crystals, whereas the

pulse wave mode produces finer equiaxed crystals. The higher the laser power, the larger the grain size and the coarser the microstructure. Moat et al. [13] investigated the influence of laser pulse length and duty cycle on multi-track residual stress distributions during laser direct metal deposition. The results demonstrate that the tensile stress gradient increases while the residual stresses decrease with the duty cycle.

During LMD, the scanning strategy plays an important role in improving the accuracy and performance of fabricated parts because of the variation in thermal behavior when different path strategies are used. Zhou et al. [14] studied the microstructure and mechanical properties of TC4 samples fabricated through LMD using different scanning strategies. They found that the one-way scanning method provides finer grains and a stronger texture index than the cross-scanning method. Moreover, the one-way scanning method has higher ultimate tensile strength and plasticity than the cross-scanning method. Wan et al. [15] found that the crystalline structure, tensile strength, and fatigue strength change with varying scanning directions. Woo et al. [19] investigated the effect of scanning patterns on different microstructural properties of ferritic and austenitic steel. In both parts, epitaxial grain expansion along the construction direction produces an equiaxed grain structure. The ferritic steel parts exhibit a preferentially tilted grain pattern in the bidirectional scanning method.

Despite the tremendous efforts of many researchers, several aspects of LMD remain poorly understood, which affects the efficiency of the products and limits the application and reliability of this technology. Therefore, further studies should be conducted to determine the potential advantages of LMD. Within this context, consideration of the influence of pulsed laser parameters and different scanning strategies on the microstructure and the mechanical and geometric properties of additively manufactured walls using LMD is a relatively new addition to this field. In this study, the LMD was utilized to fabricate 316L stainless thin-walled parts. Two strategies were used to investigate the capability of LMD: (1) changing pulsed laser parameters according to (a) different frequencies, same duty cycle, and (b) different duty cycles, same frequency; and (2) changing the path strategy (unidirectional and bidirectional scanning strategies) during pulsed laser. The microstructure and the microhardness profile of the macro cross section of the samples were characterized. This study also investigated the influence of pulsed laser parameters and scanning strategies on the geometric stability of the printed wall of the fabricated samples.

2 Experimental Procedures

2.1 Materials

AISI316L stainless steel was used as the substrate and powder materials in the experiments. The chemical composition and the mechanical and thermal properties are shown in Tables 1 and 2, respectively. The powder had a size of 45–120 μm and a spherical shape. The substrates were machined to dimensions of 120 mm \times 15 mm with a thickness of 10 mm, polished, and then cleaned carefully before LMD.

2.2 LMD Production

AISI316L LMD thin-walled parts were produced using a laser material deposition system, as illustrated in Fig. 2. The system consisted of a LaserLine diode laser generator with a 4000-W maximum power supply (Manual LDF 4000-100 VGP), a six-axis manipulator (KUKA-ZH 30/60III) that can reach 2233 mm with a total load of 65 kg and a payload of 30 kg, a Precitec laser head (YC52), and a metal powder feeder (Raychem RC-PGF-D). The metal powder was conveyed through four coaxial nozzles into the deposition point by a pressurized carrier gas (argon). Argon was also used as a shielding gas during LMD. The standoff distance of the laser head was 15 mm above the substrate, and the beam spot diameter was 2 mm.

LMD experimental work was carried out in two groups (D and F), as presented in Table 3. The process parameters, such as the laser power, scanning speed, and powder flow rate, were fixed during all experiments at 1400 W, 6 mm/s, and 8 g/min, respectively. In all experiments, the Z-increment after adding each layer was 2 mm as the manipulator robot moved up to add the next layer. Each group consisted of two sections that differed in scanning strategy (i.e., unidirectional or bidirectional), as shown in Fig. 3. In group D, the effects of the duty cycle of the pulsed laser on AISI316L LMD thin-walled parts in both scanning patterns were

Table 1 Chemical compositions of 316L stainless steel

Component element	Value (%)
Carbon, C	0.030
Chromium, Cr	17
Iron, Fe	72
Manganese, Mn	2.0
Molybdenum, Mo	2.0
Nickel, Ni	10
Phosphorus, P	0.045
Silicon, Si	1.0
Sulfur, S	0.030

Table 2 Mechanical and thermal properties

Property	Value
Yield strength (MPa)	310
Elasticity modulus (GPa)	210
Density (kg m^{-3})	7800
Specific Heat ($\text{J kg}^{-1} \text{ }^\circ\text{C}^{-1}$)	585
Laser absorption coefficient	0.6
Thermal expansion coefficient ($^\circ\text{C}^{-1}$)	0.000019

investigated. The frequency was fixed, but the duty cycles were varied in each experiment. The values of duty cycles were started from the pulse width equal to two-thirds of the pulse period (2:1), then three-quarters of the pulse period (3:1), and the last one was four-fifths of the pulse period (4:1). In group F, the effects of pulse frequency on LMD thin-walled parts in both scanning patterns were analyzed. The duty cycle was fixed, but the frequencies varied from low to high in each experiment.

The specific energy of a laser beam can be expressed as the LED, as shown in Eq. (1), which is defined as the energy input per unit area of the laser beam on the substrate (J/mm^2) [21, 22]. The laser power mode in this research is pulsed waves, and the average power can be measured by using Eq. (2). The peak power is 1400 W in all experiments. However, the average power was distinguished in group D experiments as 933.8 W (d11 and d21), 1050 W (d12 and d22), and 1120 W (d13 and d23) because of the variations in the duty cycle. The average power of group F experiments was 700 W in all experiments

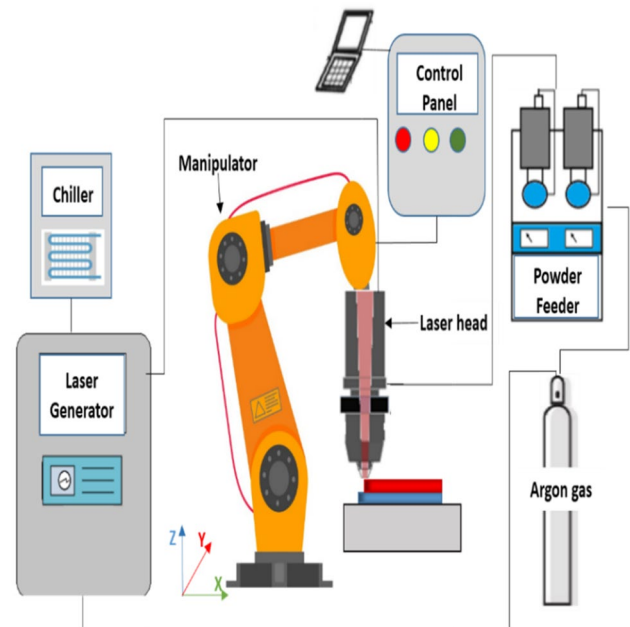


Fig. 2 Schematic of the LMD system

Table 3 Experiments groups

Group	Section	Sample name	Scanning pattern	Pulsed laser parameter			
				Frequency (Hz)	Duty cycle (%)		
D	D1	d11	Unidirectional		13.33	66.7	
		d12				75	
		d13				80	
	D2	d21	Bidirectional		13.33	66.7	
		d22				75	
		d23				80	
F	F1	f11	Unidirectional		13.33	50	
		f12					20
		f13					50
	F2	f21	Bidirectional		13.33	50	
		f22					20
		f23					50

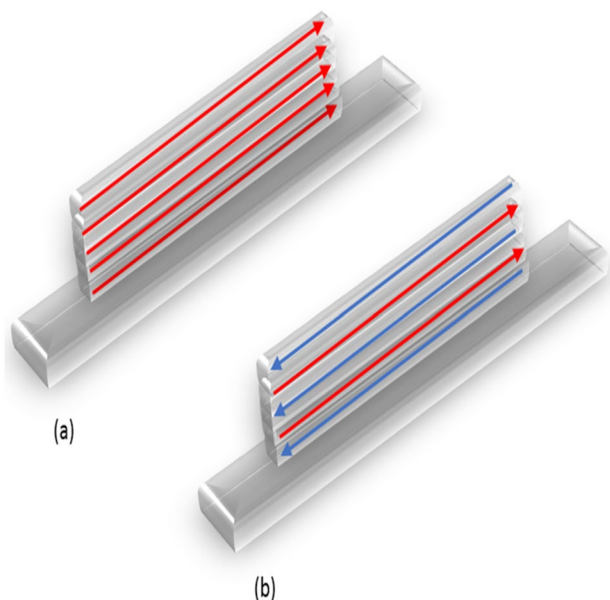


Fig. 3 Scanning pattern used in the research: **a** unidirectional (section D1 and F1 experiments), **b** bidirectional (section D2 and F2 experiments)

because the duty cycle was fixed in all experiments. Changing the pulse laser parameters can change the amount of energy distribution within the manufacturing process, as shown in Table 4, which can change the melting behavior of the material [23].

$$LED = \frac{\text{Laser Power}}{\text{Scan speed} \times \text{Beam Diameter}} \tag{1}$$

$$\text{Average Power} = \frac{\text{Duty Cycle}}{100} \times \text{Peak Power} \tag{2}$$

Table 4 Laser energy density during manufacturing

Group name	Samples	Energy density (J/mm ²)
D	d11	77.8
	d12	87
	d13	93.3
	d21	77.8
	d22	87
	d23	93.3
F	f11	58.3
	f12	58.3
	f13	58.3
	f21	58.3
	f22	58.3
	f23	58.3

2.3 Characterization Techniques

AISI316L parts were fabricated using LMD as shown in Fig. 4. They were cut from the middle and then mounted in resin. The samples were ground down from 240 to 2000 grit using SiC papers, polished, and then ultrasonically cleaned with water and alcohol. Then, the samples were etched in a saturated oxalic acid solution for microstructure analysis. The optical microscopic (OM) images were obtained under a LEICA DMi8 optical microscope at a magnification of 50 μm. The 3D measuring laser microscope OLS4000 was used to take cross-sectional images of the samples at a magnification of 800 μm. The microhardness was measured using a Vickers microhardness machine (HVS-1000Z) along with the height of samples, with a dwell period of 10 s and a test load of 200 g. The geometric properties (height, width, and depth) and grain size of the LMD-fabricated parts were measured using ImageJ software 1.53k.

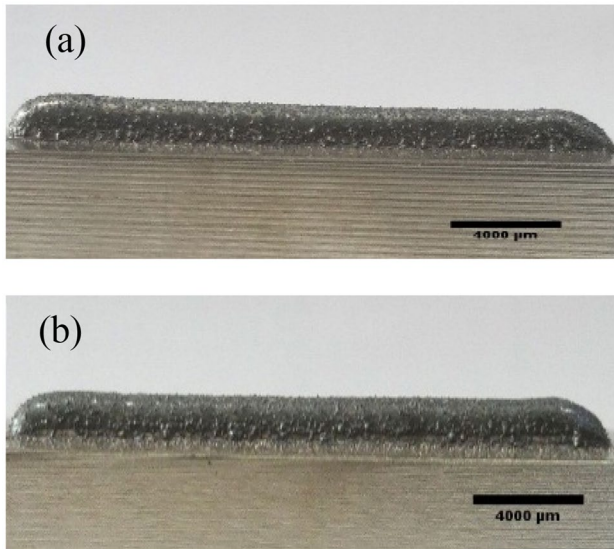


Fig. 4 LMD thin-walled samples: **a** unidirectional pattern fabricated part, **b** bidirectional pattern fabricated part

3 Results and Discussion

3.1 Geometric Properties of LMD-Fabricated Samples

Figure 5 shows the macro cross-section images of LMD thin-walled samples taken under a 3D measuring laser microscope at a magnification of 800 μm. The geometric properties (height, width, and depth) of the samples are shown in Fig. 6.

3.1.1 Impact of Pulsed Laser Parameters on the Geometric Properties of LMD-Fabricated Samples

The cross-section height, width, and depth of the LMD thin-walled parts processed by pulse laser with different parameters are listed in Table 5 and Fig. 7. These properties have been affected during the part fabrication because of the periodic characteristics of the pulse laser. As shown in Fig. 7a, b, the height and width of the parts from group D increase as the duty cycle is increased from 66.7% to 80%. This result can be ascribed to the fact that a higher duty

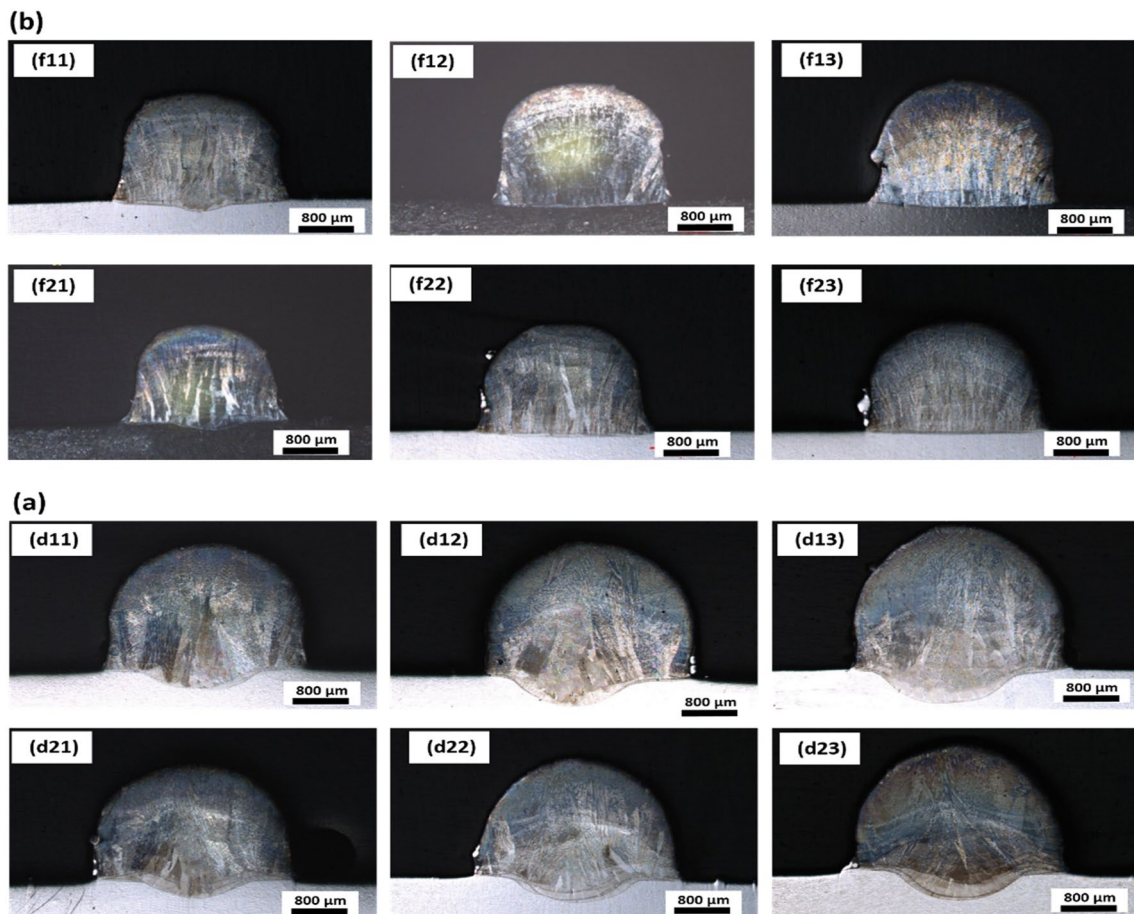


Fig. 5 Macro cross-section images of LMD thin-walled samples from **a** group D and **b** group F

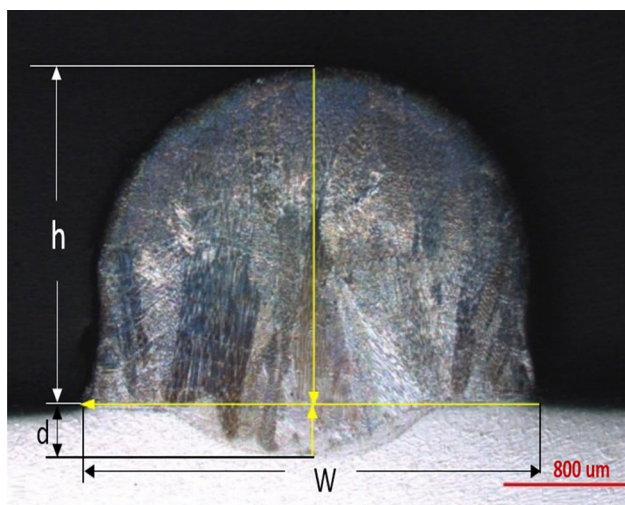


Fig. 6 Geometric properties (height, width, and depth) measured using ImageJ software

cycle corresponds to higher heat input, and the molten pool temperature can melt more metal material. Figure 7d, e show the height and width of the parts from group F with different frequencies and the same duty cycle (50%). The deposition height and width are the smallest at 13.33 Hz and the highest at 50 Hz. The height and width of the samples increase with increasing frequency. Although the heat input of the pulsed laser is the same due to the same duty cycle, the heat accumulation is different in each experiment.

Geometric stability cannot be thoroughly evaluated only by the height and width of the deposition layers. The depth is also an important index because it reflects the quality of fabricated parts and directly affects the interlayer bonding strength of formed parts. During LMD, the metal powder and substrate are heated simultaneously to form a molten pool on the substrate surface, allowing the deposited materials to mix with the substrate and create an excellent

metallurgical bond [24]. Figure 7 also presents the influence of different laser parameters on melting depth; when the duty cycle is reduced at the same frequency, the laser penetration to the substrate is reduced, as shown in Fig. 7c, because of the reduction in heat input. In contrast to the height and width of the parts from group F, the depth increases with decreasing frequency. This result is because when the frequency decreases, the laser duration in a single pulse cycle is prolonged, and the penetration into the substrate increases, as shown in Fig. 7f. The effects of the pulsed parameters, including duty cycle (D1 and D2 samples) and frequency (F1 and F2 samples), on the geometric properties of the parts are the same in the two scanning patterns (unidirectional and bidirectional). These results suggest that the geometric stability increases with increasing duty cycle but decreases with increasing frequency.

3.1.2 Impact of Scanning Pattern on the Geometric Properties of LMD-Fabricated Samples

The thin-walled parts were fabricated in this study through LMD by moving a laser beam source layer by layer to melt the feed material powder onto a substrate. The design of scanning paths is significant for optimizing the performance of manufactured samples because it changes the thermal history of each layer [25]. The samples from D1 (d11, d12, and d13) and D2 (d21, d22, and d23) only differ in scanning strategy, and other experimental parameters are unchanged. Similarly, the samples from sections F1 and F2 only differ in scanning strategy, and other experimental parameters are unchanged. Given that the unidirectional scanning pattern is used to fabricate the samples from sections D1 and F1, the deposition of the new layer starts from the starting point of the preceding one. Thus, the cooling rate of the produced layer is uniform. In addition, this scanning pattern prolongs the cooling time of the samples. The deposition pattern also affects the shape of the molten pool and temperature

Table 5 Geometric properties of LMD samples

Group name	Sample name	Scanning pattern	Height (μm)	Width (μm)	Depth (μm)
D	d11	Unidirectional	2235 ± 20	2922 ± 30	315 ± 5
	d21	Bidirectional	2065 ± 20	2798 ± 30	274 ± 5
	d12	Unidirectional	2416 ± 20	2958 ± 30	486 ± 5
	d22	Bidirectional	2132 ± 20	2833 ± 30	391 ± 5
	d13	Unidirectional	2571 ± 20	3092 ± 30	584 ± 5
	d23	Bidirectional	2236 ± 20	2961 ± 30	475 ± 5
F	f11	Unidirectional	1827 ± 20	2586 ± 30	207 ± 5
	f21	Bidirectional	1652 ± 20	2430 ± 30	185 ± 5
	f12	Unidirectional	1982 ± 20	2617 ± 30	150 ± 5
	f22	Bidirectional	1806 ± 20	2580 ± 30	114 ± 5
	f13	Unidirectional	2065 ± 20	2782 ± 30	100 ± 5
	f23	Bidirectional	1869 ± 20	2691 ± 30	77 ± 5

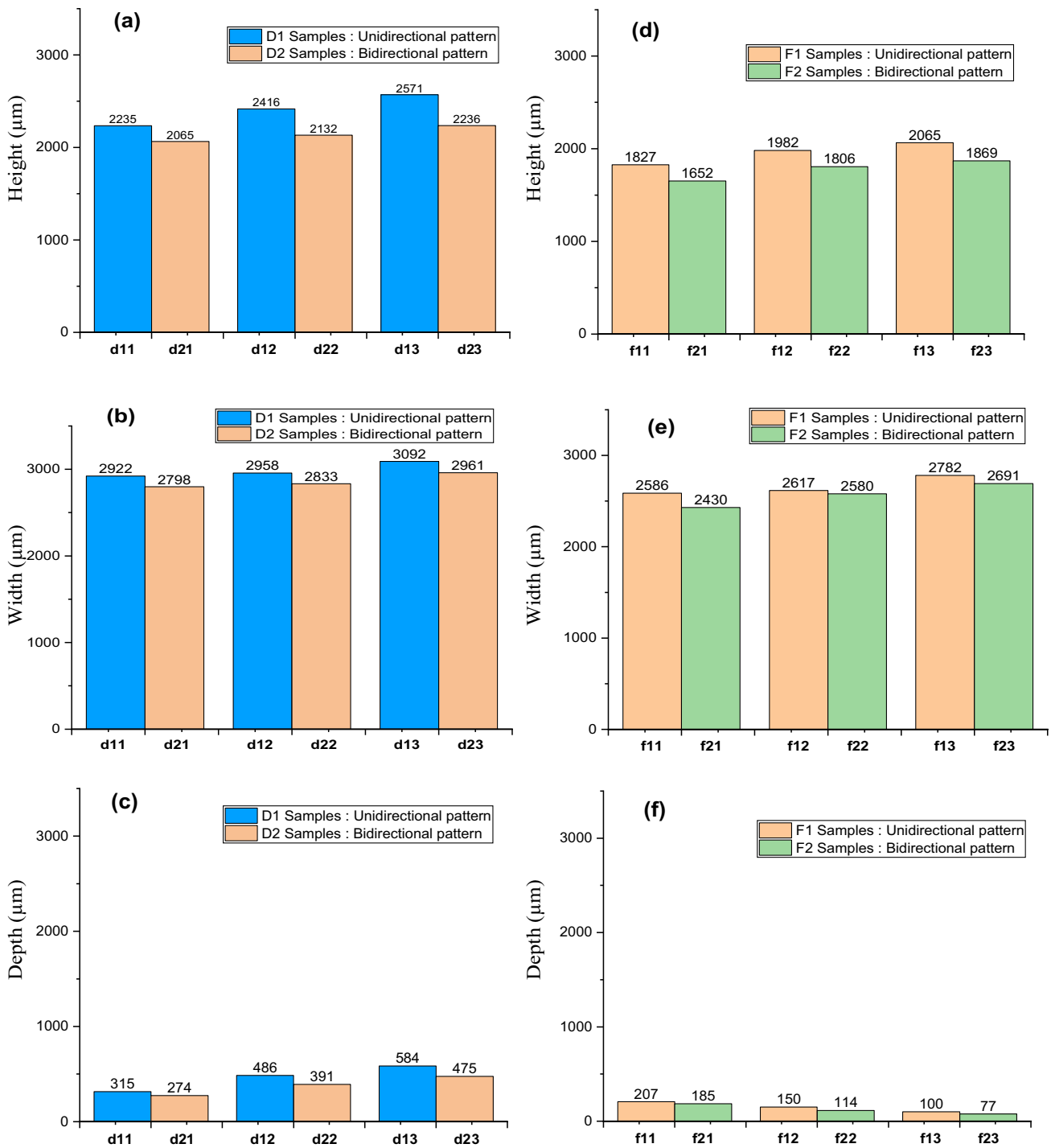


Fig. 7 Geometric properties of samples: **a**, **b**, and **c** are the height, width, and depth of group D samples, respectively; **d**, **e**, and **f** are the height, width, and depth of group F samples, respectively

gradient during LMD [26]. Thus, in a unidirectional scanning pattern, the subsequent layer is deposited on the previous one at a lower temperature, driving the thermal gradient higher. By comparison, the samples from sections D2 and F2 are produced with a bidirectional pattern, indicating that the preceding layer has a higher temperature, resulting in a low

thermal gradient. Given their longer cooling time, higher cooling rate, and higher thermal gradient, the samples from sections D1 and F1 have better surface quality than the samples from sections D2 and F2.

Moreover, the samples from sections D1 and F1 are more geometrically stable than those from sections D2 and F2 in

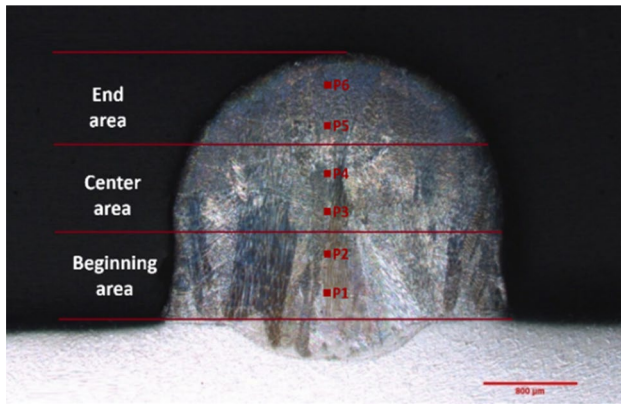


Fig. 8 Measured points of grain size in different areas in the thin-walled samples fabricated using LMD

terms of height, width, and penetration depth, as shown in Figs. 5 and 7.

3.2 Microstructure of LMD-Fabricated Samples

Metallographic images of the central region of the samples from six different zones (beginning, center, and end) are shown in Figs. 8 and 9. The laser energy is absorbed when the laser beam interacts with powder particles during LMD, causing the laser energy to attenuate. The residual laser energy reacts with the substrate surface, melting it if the laser beam energy is sufficient. Otherwise, the substrate is not melted. The same process continues when adding a new layer, with the surface of the previous layer acting as the substrate surface. This process forms a molten and recrystallized zone in the surface zone and an interlayer zone where

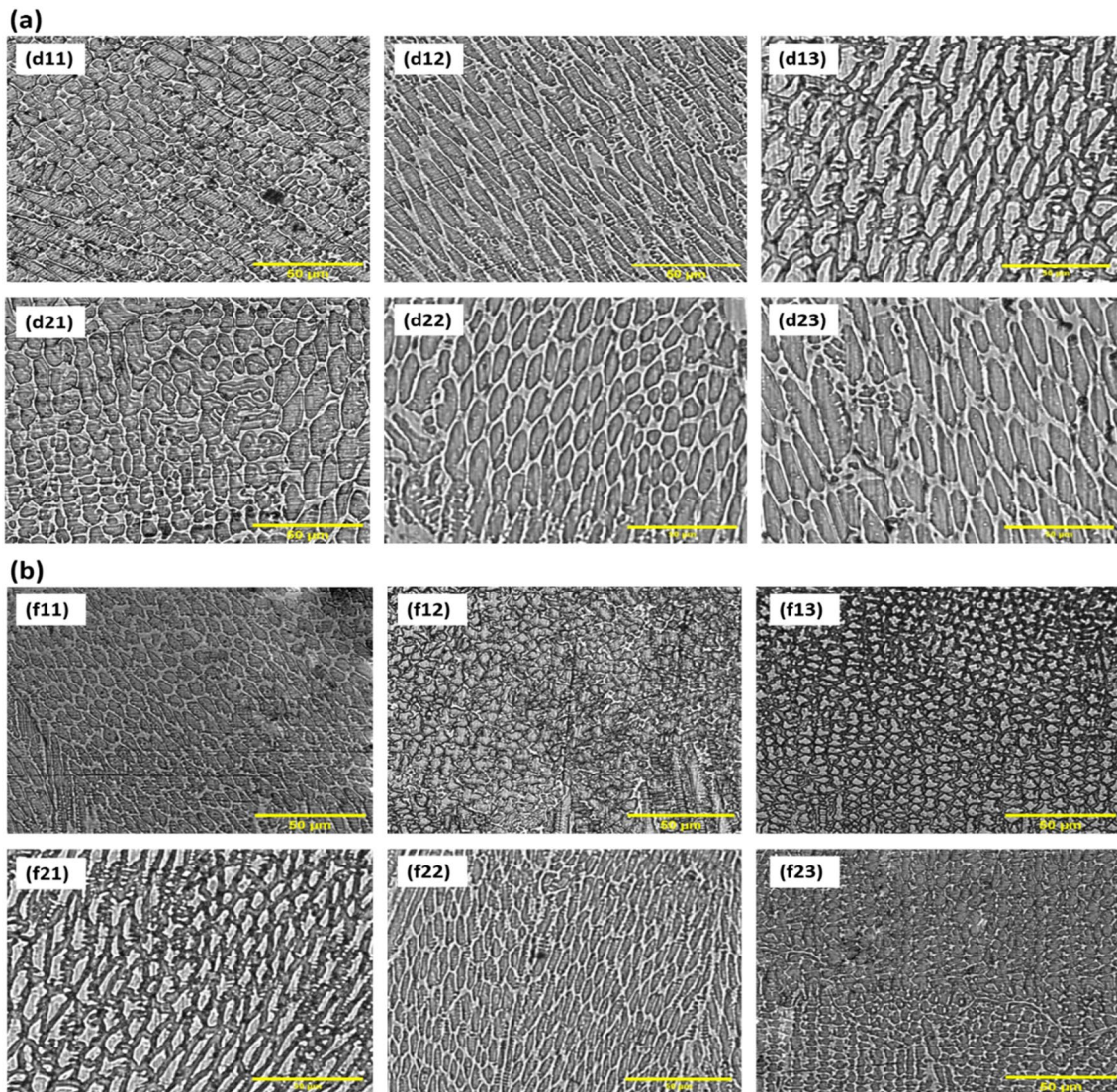


Fig. 9 Optical microscopic images of samples from **a** group D and **b** group F

the material is deposited, resulting in changes in microstructure and grain size.

3.2.1 Impact of Pulsed Laser Parameters on the Microstructure of LMD-Fabricated Samples

The microstructure morphology and grain size of the LMD-fabricated samples affect their final mechanical properties. The microstructure depends on the thermal history of the molten pool. The lower the cooling rate, the coarser the grain size and the lower the tensile strength. The temperature gradient and solidification rate affect the grain size and growth direction of the samples. Pulsed laser has the characteristics of low heat input, which makes the cooling rate of the molten pool faster and the grain finer. In addition, the solidification of the pulsed laser processing molten pool is a periodic change process.

As shown in Fig. 10, all samples from the four sections (D1, D2, F1, and F2) have a similar trend in grain size in the three regions (beginning, center, and end). However, the grain size of the samples from the same section has different values in the three regions. The grain size of the samples from section D1 is in the order of $d11 < d12 < d13$, as shown in Fig. 10a. The same pattern is observed in the samples from section D2, i.e., $d21 < d22 < d23$.

The difference in grain size is that the inputted energy in $d11$ and $d21$ is lower than that in $d12$ and $d22$, which is lower than the inputted energy in $d13$ and $d23$ because of the decreasing duty cycle. The low inputted energy contributes to the refined structure and makes the grain generated by the higher cooling rate of the molten pool smaller. Thus, the grain size increases with the increasing duty cycle from 66.7% to 80%.

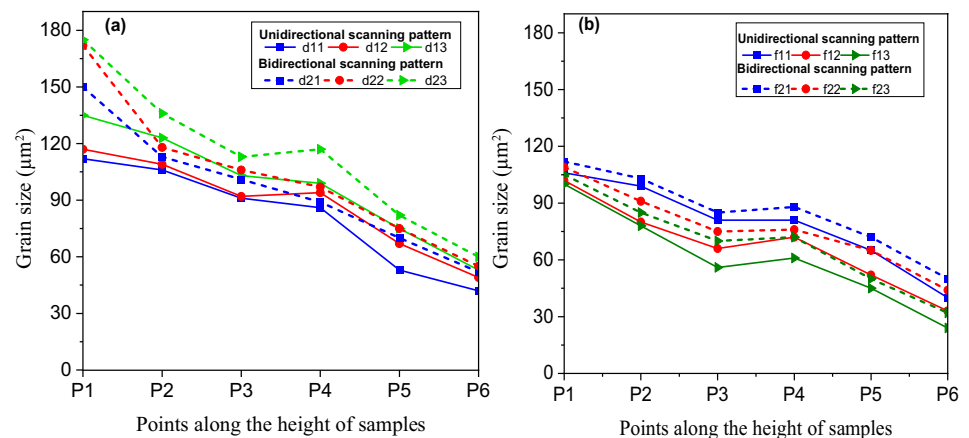
Figure 10b presents the grain size of the samples from group F. These samples differ in grain size in each zone, although the inputted power is the same in all samples. The temperature histories of the molten pools are different because of the different durations of a single pulse [27],

resulting in different energy distributions and grain sizes between the samples in section F1 ($f11$, $f12$, and $f13$) and between the samples in section F2 ($f21$, $f22$, and $f23$). The grain size is in the order of $f11 \gg f12 > f13$. The same pattern can be observed in the samples from section F2, i.e., $f21 > f22 > f23$, as illustrated in Fig. 10b. Although the duty cycle is the same in the samples from group F (50%), approximately 13 cycles per second can be found in the $f11$ and $f21$ samples, which have a 37.5 ms pulse period followed by a 37.5 ms pulse off for solidification; 20 cycles per second in the $f12$ and $f22$ samples, which have a 25 ms pulse period followed by a 25 ms pulse off for solidification; and 50 cycles per second in the $f13$ and $f23$ samples, which have a 10 ms pulse period followed by a 10 ms pulse off for solidification. The higher the single pulse energy and the fewer the pulses, the larger the grain size, as observed in the samples from $f11$ and $f21$ with a frequency of 13.33 Hz. The lower the single pulse energy and the more pulses, as shown in the samples from $f13$ and $f23$ with a frequency of 50 Hz, the smaller the grain size.

3.2.2 Impact of Scanning Pattern on the Microstructure of LMD-Fabricated Samples

Figure 10a shows the grain size of the samples from sections D1 and D2. Figure 10b shows the grain size of the samples from sections F1 and F2. The samples from sections D1 and F1 were manufactured with unidirectional scanning patterns, whereas those from D2 and F2 were manufactured with bidirectional scanning patterns. Although the two groups have different pulsed laser parameters, the influence of the scanning pattern is the same in both groups. The grain size values in the three regions show fewer differences in the D1 and F1 samples than in the D2 and F2 samples. This result can be ascribed to the fact that the cooling is more uniform throughout the samples fabricated with the unidirectional scanning pattern (D1 and F1 samples) compared with the samples fabricated with the bidirectional scanning pattern

Fig. 10 Grain size change trend diagram in LMD thin-walled samples from **a** group D and **b** group F



(D2 and F2 samples), and they have a higher cooling rate. The cooling duration is also longer in the D1 and F1 samples than in the D2 and F2 samples. When the cooling period is prolonged, the temperature decreases during the fabrication cycle, reducing the grain size in all layers. Consequently, the D1 and F1 samples have a smaller grain size than the D2 and F2 samples.

The graphs in Fig. 10 show that the grain size of the LMD-fabricated samples has been dropping from the beginning zone until the end zone. When the substrate is irradiated by the laser beam, it stores the heat and works as a heat source, which leads to the grain size of the samples from the beginning zone being much larger than those of the samples from the other zones [28]. The effect of the heat stored in the substrate decreases with the deposition of more layers as the thermal conductivity resulting from the substrate decreases, causing the grain size at the center area of the sample to decrease. The graphs show that the grain size at the top layers continues to decrease. This decrease is because the top layers are conducted with ambient air from the other side, which increases the cooling rate and solidification, causing the grain size on the top layers to decrease.

3.3 Microhardness of LMD-Fabricated Samples

Figure 11 shows a schematic of the microhardness test for the LMD-fabricated samples where the ten sampling points are carried out along the central axis of the deposited layers. Figure 12 shows the distribution curve of Vickers hardness with different pulse parameters and different scanning strategies along the central axis of the deposited layers. The graphs show that the microhardness trend is almost the same in all thin-walled samples fabricated using LMD. The figures show a higher microhardness value on the top of the

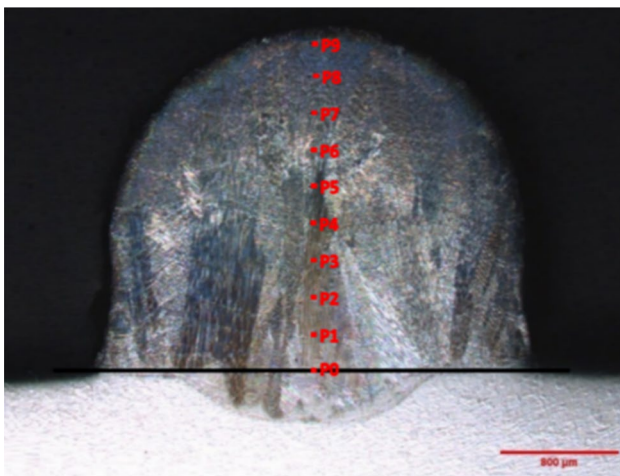


Fig. 11 Microhardness measured points in the LMD thin-walled samples

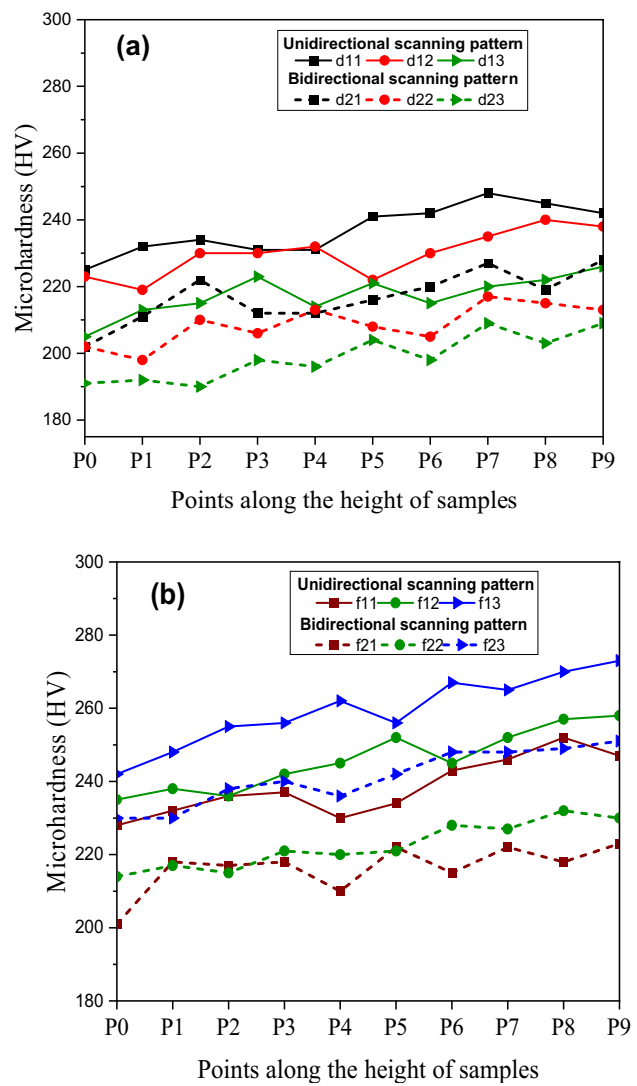


Fig. 12 Microhardness change curve of the cross section of LMD thin-walled samples from a group D and b group F

deposition, where higher cooling rates are achieved than in the center and beginning area of the deposition. As discussed in Sect. 3.2, the remelting and recrystallization of the preceding layer during the addition of a new layer in LMD alter the grain size and the microstructure of the interlayer. Moreover, the microhardness varies as a result of these changes. Furthermore, the LMD, especially in pulsed-wave mode, has a fast cooling rate of fine grain structure and produces a fine grain-strengthening effect, which can significantly improve the hardness of the deposited layers [27].

3.3.1 Impact of Pulsed Laser Parameters on the Microhardness of LMD-Fabricated Samples

The microhardness curve and the average microhardness of the samples from group D are illustrated in Figs. 12a and

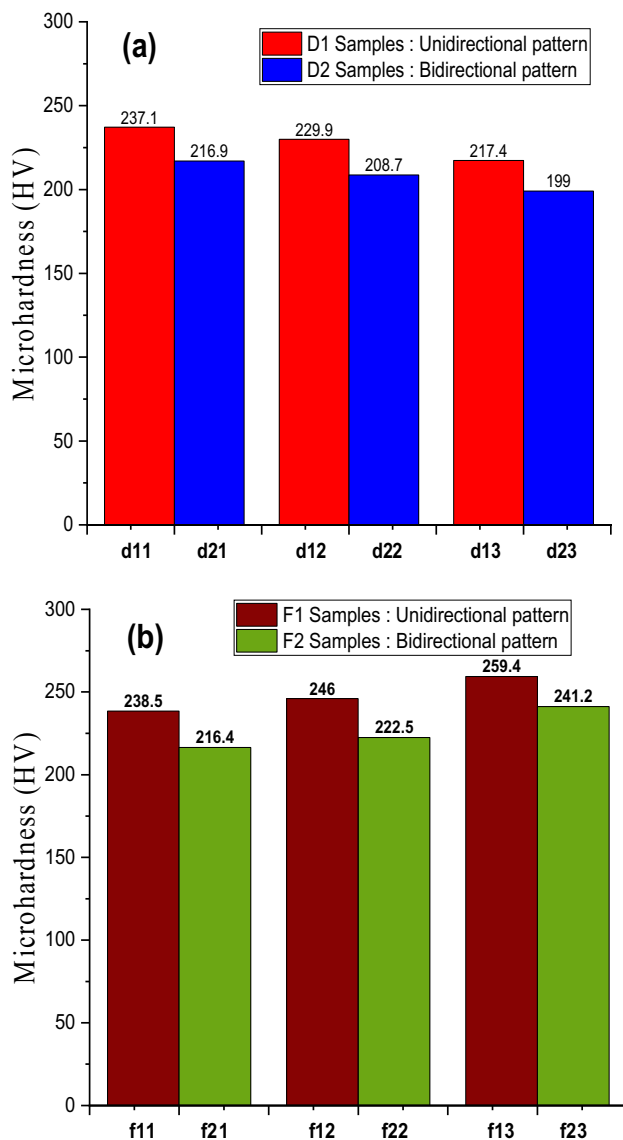


Fig. 13 Effects of pulse laser parameters and scanning pattern on the microhardness of LMD-fabricated samples from **a** group D and **b** group F

13a, respectively. They represent the significant impact of the changing duty cycle on microhardness during LMD. This variation in microhardness values is because the thermal histories of the LMD components manufactured using a pulsed laser are significantly different because of the varied energy distribution and cooling rate caused by the variation in pulsed laser parameters, which makes the grain size distinct and then affects the microhardness of LMD components. A comparison of the average microhardness of the deposition layers of different samples shows that the average microhardness gradually increases with decreasing duty cycle in both scanning strategies. In the unidirectional scanning pattern, the average microhardness values are 217.4, 229.9, and

237.1 at duty cycles of 80%, 75%, and 66.7%, respectively. In the bidirectional scanning pattern, the average microhardness values are 199, 208.7, and 216.9 at duty cycles of 80%, 75%, and 66.7%, respectively. This variation in microhardness is due to the fact that the heat input decreases with decreasing duty cycle, thereby enhancing the cooling rate, fine microstructure, and microhardness.

The effect of changing pulsed laser frequencies on the microhardness of LMD thin-walled samples is illustrated in Figs. 12b and 13b. The average microhardness gradually increases with increasing frequency during unidirectional and bidirectional scanning strategies, as shown in Fig. 13b. The pulse frequency mainly affects the cooling time. The smaller the frequency, the more sufficient the cooling of the deposition layers. The faster the cooling rate, the finer and smaller the microstructure, and the greater the microhardness.

During pulsed laser LMD, the microhardness increases as the duty cycle decreases. As shown in Sect. 3.1, when the duty cycle decreases, the inputted energy decreases, which causes the created molten pool to decrease. The smaller the molten pool, the faster it cools, which leads to smaller grains and higher microhardness [29]. This result is confirmed by the d11 and d21 samples having the highest microhardness among the samples. Although the samples from group F have the same average power (700 W), the single pulse energy is lower at 50 Hz than at 20 and 13.33 Hz, leading to a relatively higher microhardness because a faster cooling rate is maintained in the f13 and f23 samples.

3.3.2 Impact of the Scanning Pattern on the Microhardness of LMD-Fabricated Samples

The microhardness curves of the samples from groups D and F are shown in Fig. 12a, b, respectively. Despite being performed with different pulsed laser parameters (duty cycle and frequency), the impact of the scanning pattern is the same in each group. A comparison of the microhardness behavior of section D1 samples (d11, d12, and d13) that were manufactured with a unidirectional scanning strategy and section D2 samples (d21, d22, and d23) that were manufactured with a bidirectional scanning strategy shows that the samples with the same pulsed parameter and different scanning patterns [(d11 and d21), (d12 and d22), and (d13 and d23)] have similar microhardness variation trends with different values, as evidenced from the average microhardness graphs shown in Fig. 13a. The same effect of the scanning pattern is also observed in the samples from group F, as shown in Figs. 12b and 13b. These differences in microhardness values of the samples are due to the difference in microstructure grain size, as analyzed in Sect. 3.2. Compared with the D2 and F2 samples produced using a bidirectional scanning strategy, the D1 and F1 samples manufactured using

a unidirectional scanning strategy not only have a lower temperature during manufacture because of a more uniform cooling rate and longer cooling time but also possess an ultimately smaller grain size [30]. The smaller the grain size in a region, the greater its strength and hardness [31].

4 Conclusions

In this study, a thin-walled AISI316L stainless steel was fabricated through LMD using a low-power pulsed laser and two scanning patterns (unidirectional and bidirectional). This study investigated the geometric properties, microstructure, and microhardness of the samples. The major conclusions can be summarized as follows:

1. In groups D and F, the unidirectional scanning pattern shows more stability than the bidirectional scanning pattern. Higher geometric stability, smaller grain size, and higher microhardness can be acquired in the unidirectional scanning pattern than in the bidirectional scanning pattern.
2. The influence of pulsed laser parameters (duty cycle and frequency) is the same in the unidirectional and bidirectional patterns.
3. The geometric stability increases with increasing duty cycle. However, the geometric stability does not vary considerably using different frequencies.
4. The microstructure grain size is influenced by the duty cycle of the pulsed laser. The grain size increases with increasing duty cycle. The microstructure shows a smaller grain size at 66.7% in d11 and d21, and the larger grain size appears at 80% in d13 and d23. The frequency also affects the microstructure and grain size of the samples. The grain size increases with decreasing frequency; large grains appear at 13.33 Hz in the f11 and f21 samples, whereas small grains appear at 50 Hz in the f13 and f23 samples.
5. The microhardness values of the deposited layers vary considerably with the pulsed laser parameters in each zone. The average value of microhardness increases with decreasing duty cycle of pulse laser but increases with increasing frequency. The maximum microhardness values of the samples from groups D and F are presented in d11 and f13, respectively.
6. The influence of the duty cycle on geometric properties is stronger than that of frequency. However, the effect of frequency on microhardness is stronger than that of the duty cycle.

These results suggest that the pulsed laser parameters and scanning patterns considerably influence the properties of LMD-fabricated components. These parameters and patterns

must be regulated to improve the quality and efficiency of the product and the reliability of LMD.

Further studies should investigate the influence of the low-power pulsed laser parameters and scanning patterns on tensile stress, residual stress, and thermal distortion of the substrates during LMD.

Acknowledgements This research work was supported partially by the National Natural Science Foundation of China (No. 52175455), Equipment Pre-research Foundation (No. 80923010401), Science and Technology Innovation Fund of Dalian (No.2020JJ26GX040), and Fundamental Research Funds for the Central Universities (No. DUT20JC19).

Declarations

Conflict of interest The authors have no conflicts of interest to declare that are relevant to the content of this article.

Open Access This article is licensed under a Creative Commons Attribution 4.0 International License, which permits use, sharing, adaptation, distribution and reproduction in any medium or format, as long as you give appropriate credit to the original author(s) and the source, provide a link to the Creative Commons licence, and indicate if changes were made. The images or other third party material in this article are included in the article's Creative Commons licence, unless indicated otherwise in a credit line to the material. If material is not included in the article's Creative Commons licence and your intended use is not permitted by statutory regulation or exceeds the permitted use, you will need to obtain permission directly from the copyright holder. To view a copy of this licence, visit <http://creativecommons.org/licenses/by/4.0/>.

References

1. Akbari M, Kovacevic R (2018) An investigation on mechanical and microstructural properties of 316LSi parts fabricated by a robotized laser/wire direct metal deposition system. *Addit Manuf* 23:487–497
2. Eo DR, Park SH, Cho JW (2018) Inclusion evolution in additive manufactured 316L stainless steel by laser metal deposition process. *Mater Des* 155:212–219
3. Wang H, Liu W, Tang Z, Wang Y, Mei X, Saleheen KM, Wang Z, Zhang H (2020) Review on adaptive control of laser-directed energy deposition. *Opt Eng* 59(7):070901
4. Zhang K, Liu W, Shang X (2007) Research on the processing experiments of laser metal deposition shaping. *Opt Laser Technol* 39(3):549–557
5. D'Oliveira ASC, da Silva PSC, Vilar RM (2002) Microstructural features of consecutive layers of Stellite 6 deposited by laser cladding. *Surf Coat Technol* 153(2–3):203–209
6. Riquelme A, Rodrigo P, Escalera-Rodríguez MD, Rams J (2020) Additively manufactured Al/SiC cylindrical structures by laser metal deposition. *Materials* 13(15):3331
7. Xiang S, Luan H, Wu J, Yao KF, Li J, Liu X, Tian Y, Mao W, Bai H, Le G, Li Q (2019) Microstructures and mechanical properties of CrMnFeCoNi high entropy alloys fabricated using laser metal deposition technique. *J Alloys Compd* 773:387–392
8. Xue P, Zhu L, Xu P, Ren Y, Xin B, Meng G, Yang Z, Liu Z (2021) Research on process optimization and microstructure of CrCoNi medium-entropy alloy formed by laser metal deposition. *Opt Laser Technol* 142:107167
9. Gharbi M, Peyre P, Gorny C, Carin M, Morville S, Le Masson P, Carron D, Fabbro R (2014) Influence of a pulsed laser regime on

- surface finish induced by the direct metal deposition process on a Ti64 alloy. *J Mater Process Technol* 214(2):485–495
10. Li S, Xiao H, Liu K, Xiao W, Li Y, Han X, Mazumder J, Song L (2017) Melt-pool motion, temperature variation and dendritic morphology of Inconel 718 during pulsed-and continuous-wave laser additive manufacturing: a comparative study. *Mater Des* 119:351–360
 11. Pinkerton AJ, Li L (2003) An investigation of the effect of pulse frequency in laser multiple-layer cladding of stainless steel. *Appl Surf Sci* 208:405–410
 12. Ravi GA, Qiu C, Attallah MM (2016) Microstructural control in a Ti-based alloy by changing laser processing mode and power during direct laser deposition. *Mater Lett* 179:104–108
 13. Moat RJ, Pinkerton AJ, Li L, Withers PJ, Preuss M (2011) Residual stresses in laser direct metal deposited Waspaloy. *Mater Sci Eng, A* 528(6):2288–2298
 14. Zhou X, Xu D, Geng S, Fan Y, Liu M, Wang Q, Wang F (2021) Mechanical properties, corrosion behavior and cytotoxicity of Ti–6Al–4V alloy fabricated by laser metal deposition. *Mater Charact* 179:111302
 15. Wan HY, Zhou ZJ, Li CP, Chen GF, Zhang GP (2019) Effect of scanning strategy on mechanical properties of selective laser melted Inconel 718. *Mater Sci Eng A* 753:42–48
 16. Ali H, Ghadbeigi H, Mumtaz K (2018) Effect of scanning strategies on residual stress and mechanical properties of selective laser melted Ti6Al4V. *Mater Sci Eng A* 712:175–187
 17. Wan HY, Zhou ZJ, Li CP, Chen GF, Zhang GP (2018) Effect of scanning strategy on grain structure and crystallographic texture of Inconel 718 processed by selective laser melting. *J Mater Sci Technol* 34(10):1799–1804
 18. Bhardwaj T, Shukla M (2018) Effect of laser scanning strategies on texture, physical and mechanical properties of laser sintered maraging steel. *Mater Sci Eng A* 734:102–109
 19. Woo W, Kim DK, Kingston EJ, Luzin V, Salvemini F, Hill MR (2019) Effect of interlayers and scanning strategies on through-thickness residual stress distributions in additive manufactured ferritic-austenitic steel structure. *Mater Sci Eng A* 744:618–629
 20. Choi YR, Sun SD, Liu Q, Brandt M, Qian M (2020) Influence of deposition strategy on the microstructure and fatigue properties of laser metal deposited Ti–6Al–4V powder on Ti–6Al–4V substrate. *Int J Fatigue* 130:105236
 21. Liu Z, Kim H, Liu W, Cong W, Jiang Q, Zhang H (2019) Influence of energy density on macro/micro structures and mechanical properties of as-deposited Inconel 718 parts fabricated by laser engineered net shaping. *J Manuf Process* 42:96–105
 22. Pinkerton AJ, Li L (2003) The effect of laser pulse width on multiple-layer 316L steel clad microstructure and surface finish. *Appl Surf Sci* 208:411–416
 23. Mumtaz KA, Hopkinson N (2010) Selective laser melting of thin wall parts using pulse shaping. *J Mater Process Technol* 210(2):279–287
 24. Huang FX, Jiang ZH, Liu XM, Lian JS, Chen L (2011) Effects of process parameters on microstructure and hardness of layers by laser cladding. *ISIJ Int* 51(3):441–447
 25. Kudzal A, McWilliams B, Hofmeister C, Kellogg F, Yu J, Taggart-Scarff J, Liang J (2017) Effect of scan pattern on the microstructure and mechanical properties of powder bed fusion additive manufactured 17–4 stainless steel. *Mater Des* 133:205–215
 26. Shah K, Pinkerton AJ, Salman A, Li L (2010) Effects of melt pool variables and process parameters in laser direct metal deposition of aerospace alloys. *Mater Manuf Processes* 25(12):1372–1380
 27. Wang X, Deng D, Yi H, Xu H, Yang S, Zhang H (2017) Influences of pulse laser parameters on properties of AISI316L stainless steel thin-walled part by laser material deposition. *Opt Laser Technol* 92:5–14
 28. Zhan X, Qi C, Gao Z, Tian D, Wang Z (2019) The influence of heat input on microstructure and porosity during laser cladding of Invar alloy. *Opt Laser Technol* 113:453–461
 29. Mahamood RM, Akinlabi ET, Akinlabi S (2015) Laser power and scanning speed influence on the mechanical property of laser metal deposited titanium-alloy. *Lasers Manuf Mater Process* 2(1):43–55
 30. Dezfoli ARA, Hwang WS, Huang WC, Tsai TW (2017) Determination and controlling of grain structure of metals after laser incidence: theoretical approach. *Sci Rep* 7(1):1–11
 31. Asghari-Rad P, Sathiyamoorthi P, Bae JW, Moon J, Park JM, Zargaran A, Kim HS (2019) Effect of grain size on the tensile behavior of V10Cr15Mn5Fe35Co10Ni25 high entropy alloy. *Mater Sci Eng A* 744:610–617